Inorganic Chemistry

ARTICLE

pubs.acs.org/IC

Single-Stranded Oligonucleotide Adducts Formed by Pt Complexes Favoring Left-Handed Base Canting: Steric Effect of Flanking Residues and Relevance to DNA Adducts Formed by Pt Anticancer Drugs

Jamil S. Saad,[*,†,‡,∥] Patricia A. Marzilli,[†,‡] Francesco P. Intini,[§] Giovanni Natile,[§] and Luigi G. Marzilli[*,†,‡]

[†]Department of Chemistry, Louisiana State University, Baton Rouge, Louisiana 70803, United States

[‡]Emory University, Atlanta, Georgia 30322, United States

[§]Dipartimento Farmaco-Chimico, Università di Bari, Via E. Orabona, 4, 70125 Bari, Italy

Supporting Information

ABSTRACT: Platinum anticancer drug binding to DNA creates large distortions in the cross-link (G*G*) and the adjacent XG* base pair (bp) steps (G* = N7-platinated G). These distortions, which are responsible for anticancer activity, depend on features of the duplex (e.g., base pairing) and of the cross-link moiety (e.g., the position and canting of the G* bases). The duplex structure stabilizes the head-to-head (HH) over the head-to-tail (HT) orientation and right-handed (R) over left-handed (L) canting of the G* bases. To provide fundamental chemical information relevant to the assessment of such duplex effects, we examine (*S,R,R,S*)-**Bip**Pt(oligo) adducts (**Bip** = 2,2′-bipiperidine with *S,R,R,S* chiral centers at the N, C, C, and N chelate ring atoms, respectively; oligo = d(G*pG*) with 3′- and/or 5′-substituents). The moderately bulky (*S,R,R,S*)-**Bip** ligand favors L canting and slows rotation about the Pt−G* bonds, and the (*S,R,R,S*)-**Bip**Pt(oligo) models provide more useful data than do dynamic models derived from active Pt drugs. All 5′-substituents in (*S,R,R,S*)-**Bip**Pt(oligo) adducts favor the normal HH conformer (∼97%) by destabilizing the HT conformer through clashes with the 3′-G* residue rather than through favorable H-bonding interactions with the carrier ligand in the HH conformer. For all (*S,R,R,S*)-**Bip**Pt(oligo) adducts, the S pucker of the 5′-X residue is retained. For these adducts, a 5′-substituent had only modest effects on the degree of L canting for the (*S,R,R,S*)-**Bip**Pt(oligo) HH conformer. This small flanking 5′-substituent effect on an L-canted HH conformer contrasts with the significant decrease in the degree of R canting previously observed for flanking 5′-substituents in the R-canted (*R,S,S,R*)-**Bip**Pt(oligo) analogues. The present data support our earlier hypothesis that the distortion distinctive to the XG* bp step (S to N pucker change and movement of the X residue) is required for normal stacking and X·X′ WC H bonding and to prevent XG* residue clashes.

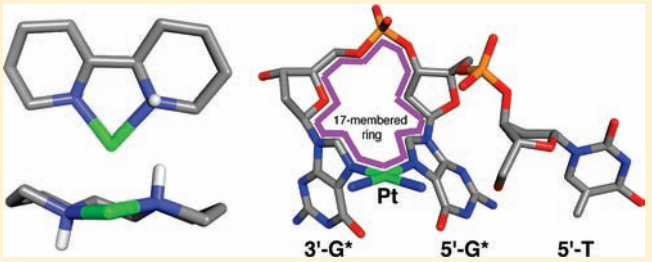

INTRODUCTION

Cisplatin and related Pt anticancer drugs form several classes of DNA adducts.[1−3] In the most readily formed adduct, Pt binds at the N7 atoms of adjacent G residues (Figure 1) to form an intrastrand cross-link lesion with a 17-membered Pt(d(G*pG*)) macrocyclic ring (asterisk indicates that N7 is bound to Pt, Figure 2).[1−10] In duplexes the G*G* cross-link exists primarily as the HH1 conformer, which has head-to-head bases, anti G* residues, and a sugar−phosphate backbone propagating in the normal direction, i.e., with Pt to the rear, the progression from 5′ to 3′ along the backbone is clockwise in HH1 (Figure 1). A long-recognized consequence of formation of this ring is the distortion of the G*G* base-pair (bp) step, featuring unstacking of the bases and changes in G* base canting.[11−13]

More recently, NMR and X-ray studies of duplex oligomers containing the intrastrand cisplatin lesion[14,15] (and an oligomer adduct of a rather bulky monofunctional Pt anticancer agent[16,17]) have all revealed a similar and unusual location of the bp adjacent to the 5′-G* bp. Our solution studies[14] established that this unusual XG* bp step exists in solution for most duplexes with a G*G* and A*G* intrastrand cross-link; the latter is the second most abundant lesion.[18] The distorted XG* bp step is also present in an HMG-bound duplex cross-link adduct in the solid state.[15] Thus, both the XG* and the G*G* bp steps are distorted, and the distortion of the XG* bp step may be even more important in anticancer activity than the distortion in the G*G* bp step. Our studies thus far have suggested to us that steric effects cause the XG* distortion.[19,20] We concluded that despite the small size of the ammonia ligand of a G*G* intrastrand cross-link formed by cisplatin, the restraints imposed by the sugar−phosphate backbone lead to large interligand interactions of ammonia with the X residue.[19] The positions of these X, 5′-G*, and 3′-G* residues (and hence the distortions) are modulated by the canting of the G* bases in the cross-link.

Received: May 31, 2011
Published: August 05, 2011

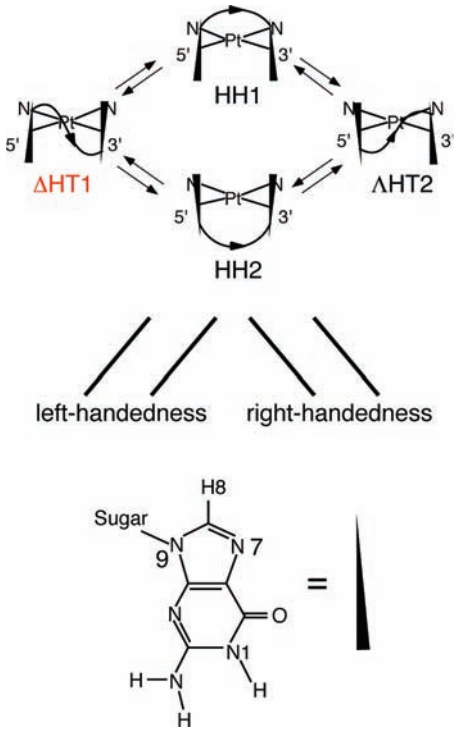

Figure 1. (Top) Four possible conformers of adducts containing the Pt(d(G*pG*)) macrocyclic chelate ring. G* base (bottom) is depicted as a black triangle with five- and six-membered rings at the tip and base, respectively. 3′-G* residue has the syn conformation in the ΔHT1 conformer. All other residues are anti. Right (R) and left (L) canting of bases (middle) is shown. Canting direction is independent of the HH or HT base orientation. For simpler models with unlinked bases, the HT chirality is defined as in this figure, but in general there is only one HH conformer. The conformer designation and some data for the ΔHT1 conformer in this and other figures are color-coded red.

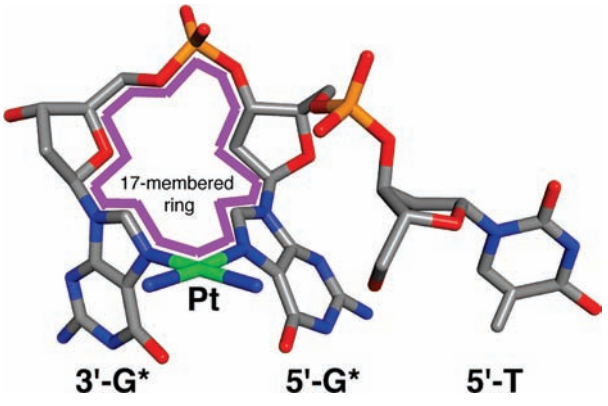

Figure 2. Representative structure of the Pt(G*pG*) cross-link. Pt links adjacent G* residues to form the typical HH1 conformer. The view was chosen to show the anti conformation of the G* residues and the 17-membered chelate ring (outlined in purple) in an HH1 G*G* lesion. [The figure was generated by PyMOL (www.pymol.org) by using molecule L1, one of the three *cis*-Pt(NH$_3$)$_2$(d(CG*G*)) structures characterized by X-ray crystallography.[25] The cytosine residue has been converted to a thymine.].

Several interesting features distinguish the XG* step. First, the step has a large positive slide and shift.[14,15] Second, the sugar in the X residue has an N pucker,[13−15] which may either cause the distortion exemplified by the XG* bp step or be a consequence of the essentially normal X·X′ Watson−Crick (WC) H bonding (X·X′ is the 5′-flanking base pair).[14,15] Finally, forces within duplexes having this XG* bp step cause the canting of the G* bases in the G*G* bp step to be low. Canting has two components: direction [(L) left- or (R) right-handed, Figure 1] and degree [departure of base plane from 90° with respect to coordination plane]. A low degree of R canting is favored by Pt duplex adducts.[13,14,21,22] However, single-strand (ss) adducts have a high degree of L canting.[23,24] In a solid-state structure of a left-handed cross-link model, one NH in the ligand cis to the canted 5′-G* always has an H bond to the oligo,[11,25] and the X residue sugar has an S pucker.[25]

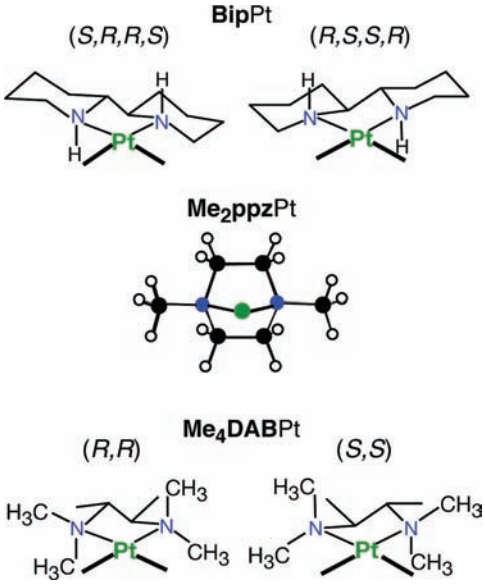

Figure 3. (Top) **Bip**Pt moiety with *R,S,S,R* or *S,R,R,S* chirality (stereochemistry defined for the N, C, C, and N ring atoms of the carrier-ligand backbone). (Middle) Ball-and-stick figure of the **Me$_2$ppz**Pt moiety. These moieties have moderate bulk. (Bottom) **Me$_4$DAB**Pt moiety with *S,S* or *R,R* chirality (stereochemistry defined for the carbon chelate ring atoms of the carrier ligand). This moiety has large bulk.

Assessment of the structural properties of *cis*-Pt(NH$_3$)$_2$(d(G*pG*)) and *cis*-Pt(NH$_3$)$_2$(oligo) ss adducts by using ^{1}H NMR data is less clear than might be expected from their simplicity because these models suffer from what we call the 'dynamic motion problem'.[13,26−29] Specifically, ^{1}H NMR data for these *cis*-Pt(NH$_3$)$_2$ models can be attributed to a single conformer or to a mixture of rapidly interconverting conformers. The observation of only one signal for each type of proton in spectra of the *cis*-Pt(NH$_3$)$_2$**G**$_2$ (**G** = unlinked monodentate guanine derivative)[30,31] and *cis*-Pt(NH$_3$)$_2$(d(G*pG*)) adducts[23,32] led to two different interpretations. The unlinked models are believed to exist as a mixture of conformers rapidly interconverting via Pt−**G** N7 bond rotation.[31] However, essentially only the HH1 conformer (Figures 1 and 2) has been implicit in reports analyzing the data for the *cis*-Pt(NH$_3$)$_2$(d(G*pG*)) complex.[11,18,22−24,32−34]

To assess better the G* base orientation and the ease of Pt−G* N7 bond rotation in the large Pt(d(G*pG*)) macrocyclic rings, we employed carrier (nonleaving) ligands designed to have features that slow rotation by destabilizing the transition state

dx.doi.org/10.1021/ic2011716 |*Inorg. Chem.* 2011, 50, 8608–8620

for Pt−**G** N7 bond rotation[13,26,29,35−40] (by about a millionfold: ∼1 h half-lives vs <1 ms for analogous cisplatin derivatives[41]). Carrier ligands that simultaneously facilitate interpretation of structurally informative spectral properties and permit the coexistence of multiple conformers span a range of bulk.[5,19,20,26−29,42] The initial very informative adducts we studied contain the moderately bulky chiral carrier ligand, 2,2′-bipiperidine (**Bip**).[19,26−28,35,41,43] *Note that we designate bidentate carrier ligands in boldface type*. When coordinated, the **Bip** ligand has two energetically favored C_2-symmetrical geometries, with *S,R,R,S* or *R,S,S,R* configurations at the asymmetric N, C, C, and N chelate ring atoms (Figure 3). The asymmetric N's each have as substituents an NH group fixed in a specified position and a piperidine methylene group hindering rotation by clashing with the guanine O6 as the base rotates toward the coordination plane. The conformer distribution and chirality of the dominant HT conformer of **Bip**Pt**G**$_2$ adducts depend on the chirality of the **Bip** ligand because the N-substituent positions are interchanged in the two **Bip** enantiomers.[19,26,35,41] The **Bip** ligand chirality also influences the R- or L-canting direction (Figure 1).

In addition to the well-known HH1 conformer, a new conformer (HH2, Figure 1) was discovered for (*R,S,S,R*)-**Bip**Pt(d(G*pG*)).[26] Compared to HH1, HH2 has the opposite direction of propagation of the phosphodiester backbone with respect to the 5′-G* (with Pt to the rear, the progression from 5′ to 3′ along the backbone is clockwise in HH1 and counterclockwise in HH2). Both conformers have R canting (Figure 1).[26] The (*S,R,R,S*)-**Bip**Pt(d(G*pG*)) complex, bearing the enantiomeric **Bip** ligand (Figure 3), also showed two conformers (HH1 and ΔHT1, Figure 1);[27] these conformers have L canting. These discoveries of two conformers for each adduct marked the first reported characterizations of conformers other than HH1 for **L**Pt(d(G*pG*)) complexes (**L** = bidentate or two cis monodentate ligands). Moreover, later work employing **L** with bulk either lower or greater than **Bip** indicated that most often three conformers (HH1, HH2, and ΔHT1) exist for many **L**Pt(d(G*pG*)) adducts.[5,29,42,44]

Although **L** bulk does not modify the sugar−phosphate backbone structure in **L**Pt(d(G*pG*)) adducts, the greater clashes of larger **L** with the G* bases can introduce sufficient energy penalties to influence the degree of G* base canting.[5,26,27,29,42,44] NMR data on well-studied nondynamic **L**Pt(d(G*pG*)) adducts provide evidence for significant base canting only in the cases of the **Bip**Pt(d(G*pG*)) adducts, the only such adducts with NH groups.[26,27] The HH conformers of the **Bip**Pt(d(G*pG*)) adducts have one G* base highly canted in the direction allowing NH-to-G* O6 H bonding.[19,26−28] The lack of significant canting for most **L**, combined with its occurrence only for moderately bulky **Bip** ligands with NH groups, led to the conclusions that canting is not an intrinsic characteristic of the G* bases in the macrocyclic ring and that H bonding of the O6 to an NH group is needed for significant canting to occur.[44]

The flanking residues play a significant role in influencing the distortions in duplexes.[19,20] These 5′- and 3′-flanking residues can be viewed as substituents on the Pt(d(G*pG*)) macrocyclic chelate ring, Figure 2. Our approach to elucidating the effects of the flanking residues includes studying **L**Pt(oligo) adducts with **L** for which studies exist on the adducts of the unsubstituted Pt(d(G*pG*)) macrocycle. Previous **L**Pt(oligo) studies[19,20] build on **Me$_2$ppz**Pt(d(G*pG*)) (**Me$_2$ppz** = *N,N′*-dimethylpiperazine, Figure 3) and (*R,S,S,R*)-**Bip**Pt(d(G*pG*)) adducts.[26,29]

In the slightly L-canted **Me$_2$ppz**Pt(oligo) adducts, in which the carrier ligand has moderate bulk, the presence of flanking 5′-residues increased the degree of L canting of the HH1 conformer.[20] The effect clearly depended on the 5′-substituent steric bulk, not on N−H hydrogen bonding because **Me$_2$ppz** has no NH groups. Likewise, for R-canted (*R,S,S,R*)-**Bip**Pt(oligo) adducts, the presence of flanking 5′-residues decreased the degree of canting (i.e., L canting increases).[19] In dynamic adducts derived from active anticancer drugs, addition of flanking 5′-residues causes characteristic shifts in the G* H8 signals consistent with an increase in an L-canted HH1 conformer.[45−47]

The results of the previous investigations implied that an L-canted G*G* moiety in a duplex would be sterically unfavorable when the X base was positioned for WC base pairing. However, no previously studied nondynamic **L**Pt(oligo) model has both carrier-ligand NH groups and L canting, two characteristic features of dynamic ss adducts derived from Pt anticancer drugs. The nondynamic (*S,R,R,S*)-**Bip**Pt(oligo) adducts reported here *do possess these two characteristics*. The substituent effects in these new models are expected to reflect more faithfully substituent effects in more difficult to evaluate dynamic models derived from active drugs.

EXPERIMENTAL SECTION

Materials. The (*S,R,R,S*)-**Bip**Pt(NO$_3$)$_2$ complex was prepared as reported.[35] Oligonucleotides, synthesized by the Microchemical Facility at Emory University, were purified by fast performance liquid chromatography (FPLC). Failed sequences were removed by using ion-exchange chromatography using a Mono Q column (GE Healthcare) (A = 2 M NaCl, B = H_2O, 0−30% A over ∼105 min). Collected fractions were desalted with a Hi-Trap desalting column (GE Healthcare) (A = H_2O, 4.5 mL/min for 20 min), taken to dryness by rotary evaporation, and then dissolved in ∼0.5−1.0 mL of D_2O.

NMR spectra were obtained on a Varian (Unity or Inova) 600 MHz and Bruker Avance II (700 MHz ^{1}H) spectrometer equipped with a cryoprobe, processed with Felix (San Diego, CA) or NMRPIPE,[48] and analyzed with NMRVIEW.[49] The 2D phase-sensitive NOESY (mixing time = 500 ms) and COSY spectra were performed at 5 or 10 °C and pH ≈ 4. The decoupled ^{1}H−^{13}C heteronuclear multiple quantum coherence (HMQC) data were collected at 25 °C. The ^{31}P NMR spectra were referenced to external trimethyl phosphate (TMP). Relative percentages of conformers were calculated by using G* H8 signals. For temperature-dependence experiments, samples were heated in H_2O to avoid C8H to C8D exchange.

Preparation of Platinated Oligonucleotides (oligos). Typically, a sample (∼1−2 mM) of a given oligo was prepared in D_2O (∼1 mL). Oligo ε_{260} values were calculated[50] to be 30.1, 46.3, 29.1, 45.3, 37.6, 46.3, and 30.1 cm^{-1} mM^{-1} for d(GGT), d(GGTTT), d(TGG), d(TTTGG), d(TGGT), d(pGGTTT), and d(HxapGGT) [hexylamine-pGGT], respectively. (Note that, in addition to Hxap, the 5′-phosphate group and the phosphodiester linkage in dinucleotides only are denoted as p.) Addition of the appropriate volume of a [(*S,R,R,S*)-**Bip**Pt(NO$_3$)$_2$] solution (∼2.5 mM) to this solution to give a 1:1 stoichiometry initiated the reaction. The reaction mixtures (pH ≈4, uncorrected, ∼5°) were monitored by using G* H8 NMR signals until the reaction was complete, as indicated by the disappearance of the free d(GpG) H8 signals. Next, the pH was lowered to ∼1.3−1.7. The absence of significant chemical shift changes for the G* H8 signals with pH change confirmed Pt−G N7 binding.[30,51]

RESULTS

Signal Assignments, Determination of Conformation, and General Observations. Signal assignments (Table 1) and conformer determination (Figure 1) for [(*S,R,R,S*)-**Bip**Pt(oligo) adducts were achieved by collecting a set of 1D and 2D NMR

Table 1. ^{1}H and ^{31}P NMR Signal Assignments for the HH1 Conformer of (*S,R,R,S*)-BipPt(oligo) Adducts[a]

	5′-G*[b]							3′-G*[b]							
adduct	H8	H1′	H2′	H2″	$J_{H1'H2'}$/ $J_{H1'-H2''}$	H3′	H4′	H8	H1′	H2′	H2″	$J_{H1'H2'}$/ $J_{H1'-H2''}$	H3′	H4′	^{31}P
d(G*pG*)[c]	7.88	5.92	2.28	2.71	0/7.1	4.99	4.01	9.11	6.27	2.77	2.48	9.6/4.2	4.71	4.21	−2.80
d(TG*G*T)	8.13	6.07	2.25	2.76	*d*	5.24	4.20	9.16	6.20	2.82	2.70	9.9/4.7	5.03	4.44	−2.83
d(TG*G*)	8.14	6.08	2.25	2.76	0/7.0	5.16	4.19	9.14	6.29	2.81	2.52	9.7/4.8	4.74	4.11	−2.73
d(TTTG*G*)	8.08	6.09	2.07	2.66	*e*	4.57	4.20	9.16	6.48	2.77	2.59	9.5/5.1	4.77	4.20	−2.30
d(G*G*T)	7.92	6.06	2.29	2.74	0/7.6	5.00	4.09	9.17	6.23	2.81	2.70	8.9/4.7	5.07	4.41	−2.63
d(G*G*TTT)	7.97	6.08	2.32	2.75	0/7.6	5.06	4.09	9.17	6.19	2.78	2.66	*d*	5.05	4.40	−2.55
d(pG*G*TTT)	8.25	6.17	2.30	2.73	0/7.7	5.07	4.08	9.16	6.13	2.74	2.62	9.3/5.0	5.00	4.14	−2.98
d(HxapG*G*T)	8.17	6.15			0/7.8			9.20	6.22			9.6/4.7			−3.11

[a] NOESY and COSY experiments conducted at 5 or 10 °C, pH ≈ 4. Under these conditions, H8 signals for the free oligos range from 7.79 to 8.26 ppm. [b] Anti,anti conformational assignment based on NOE cross-peaks between H8 resonances and sugar signals. [c] Reference 27. [d] Not determined because of broadness. [e] Could not be measured because of overlap with T H1′ signals.

experiments. NOESY, COSY, HMQC, and ^{31}P NMR data were used to assess structural features. Briefly, an H8−H8 NOE cross-peak is characteristic of an HH conformer, whereas the absence of such a cross-peak is indicative of an HT conformer.[5,19,20,26,27,29,42,44] For typical **L**Pt(d(G*pG*)) and **L**Pt(oligo) complexes, HH conformers exhibit H8 and ^{31}P NMR signals more downfield than those of the free oligo[23,32,45,52−54] whereas HT conformers have more upfield-shifted H8 and ^{31}P NMR signals.[5,27−29,42,44] Intraresidue H8−H3′ NOE cross-peaks are characteristically observed for N sugars but not for S sugars.[55] Sugar conformations were also deduced from H1′ coupling patterns.[56] Strong H8−H2′/H2″ and weak (or unobservable) H8−H1′ intraresidue NOE cross-peaks are characteristic of anti residues, while strong H8−H1′ intraresidue NOE cross-peaks are typically found for syn residues.[27−29,42,44,55,57,58] For unplatinated DNA molecules, a downfield H2′ shift (~3.3 vs ~2.7 ppm) has been reported to be characteristic of the syn conformation.[59] Interestingly, the 3′-G* H2′ signal for the HT conformer for all adducts studied here is shifted significantly downfield (~3.3 ppm). This downfield H2′ shift has also been observed for the ΔHT1 3′-G* residue in many other adducts.[5,20,27,29,42,44]

In the Results section, all solutions were at pH ≈ 4 unless otherwise noted. For each (*S,R,R,S*)-**Bip**Pt(oligo) complex, we present general conformer features found by 1D NMR spectroscopy (^{1}H and ^{31}P). (G H8 and T H6 shifts of free oligos and a complete description of conformer assignments can be found in the Supporting Information.) ^{31}P NMR signals were assigned by using the above empirical relationships and the relative signal intensity compared to the conformer distribution established by 1D ^{1}H NMR spectroscopy. ^{31}P NMR spectra were recorded frequently for all samples soon after reaction completion until equilibrium was reached. ^{31}P NMR signals of phosphodiester groups linking a T residue to a G* or to another T residue and within the normal range (from ca. −3.7 to −3.9 ppm) were not assigned and are not described in this work. Because our experience indicates that ^{31}P NMR signal intensities are less reliable than H8 signal intensities, quantitative measurements of conformer abundance rely on the H8 signal intensities.

Unless stated otherwise, three new pairs of G* H8 signals were observed. Both signals of one pair are from the ΔHT1 conformer and had shifts similar to those of the free oligo. Both signals of another pair were well downfield from the H8 signals of the free oligo G. This pair of downfield signals typically disappeared in 1−2 days; the signals are thus from an unstable product that is

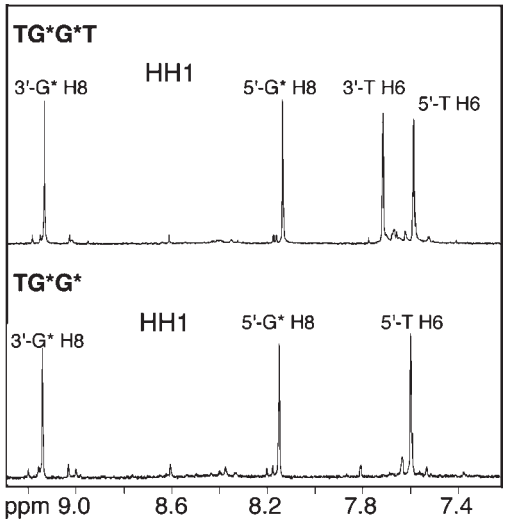

Figure 4. G* H8/T H6 region of 1D NMR spectra for (*S,R,R,S*)-**Bip**Pt(d(TG*G*T)) and (*S,R,R,S*)-**Bip**Pt(d(TG*G*)) at equilibrium (25 days, pH 4.0, 23 °C).

most probably the HH2 conformer. One H8 of the third pair has a downfield shift; the other H8 has a shift similar to the H8 shift typical of an unplatinated G. This pair is from the HH1 conformer, and the H8 shift pattern is characteristic of L canting. Reactions occurred over hours or days and were not monitored continuously. The observations described below (such as the time noted when signals appeared) reflect the availability of instrument time and provide a sense of the rate of the various reactions. Selected figures and tables of NMR data of the adducts not included in the text are presented in the Supporting Information.

(*S,R,R,S*)-BipPt(d(TG*G*T)). We describe in detail our NMR analysis of this adduct; studies on the other adducts are described below in much less detail. At 15 min after initiation of the reaction of d(TGGT) with (*S,R,R,S*)-[**Bip**Pt(NO_3)$_2$] at pH 4, three new pairs of G* H8 signals were observed (Supporting Information). Two pairs of H8 signals were downfield from the G H8 signals of free d(TGGT); the third pair, with more upfield shifts, had signals slightly downfield from those of the free d(TGGT). After 1 day, the reaction was complete and one of the new pairs of downfield H8 signals (at 8.70 and 8.85 ppm) had become barely visible. At 1 day, two abundant conformers with a

dx.doi.org/10.1021/ic2011716 |*Inorg. Chem.* 2011, 50, 8608–8620

~1:1 distribution were present (Supporting Information). Utilizing many spectral features detailed below, we determined that these two conformers are HH1 and ΔHT1. With additional time, the intensity of the ΔHT1 relatively upfield G* H8 signals decreased, until the signals were barely visible after 20 days (Figure 4 and Supporting Information). The final distribution was 96% HH1:4% ΔHT1. Thus, both the very unstable short-lived conformer with downfield G* H8 signals at 8.70 and 8.85 ppm (most likely the HH2 conformer, see below) and the unstable longer-lived ΔHT1 conformer are kinetically favored products.

2D NOESY and COSY spectra obtained for the 1-day (*S,R,R,S*)-**Bip**Pt(d(TG*G*T)) sample allowed us to assess the two abundant conformers. An NOE cross-peak is clearly observed between the two H8 signals at 8.13 and 9.16 ppm, indicating that the G* bases for this stable abundant conformer are in an HH orientation (Supporting Information).[19,20,26,27,29,42] The more downfield H8 signal (9.16 ppm) showed NOE cross-peaks with signals at 2.70 and 2.82 ppm; the latter cross-peak was the stronger of the two. Both of these peaks (at 2.70 and 2.82 ppm) showed NOE cross-peaks with a signal at 6.20 ppm; the 6.20−2.70 ppm cross-peak was stronger than the 6.20−2.82 ppm cross-peak. The signals at 2.70 and 2.82 ppm were connected to signals at 4.44 and 5.03 ppm in the NOESY spectrum. From these observations, the H1′, H2′, H2″, H3′, and H4′ signals were assigned (Table 1). The observed H8−H2′/H2″ NOE's and the absence of an observable H8−H1′ NOE are consistent with the anti nucleotide conformation.[55,57,58] The absence of an observable H8−H3′ NOE suggests that the sugar of this residue retains the S-sugar pucker;[55] therefore, these signals are assigned to the 3′-G* residue because the S pucker is characteristic of the 3′-G* residue.

The other H8 signal (at 8.13 ppm) of the stable abundant conformer showed strong NOE cross-peaks to resonances at 2.25 and 5.24 ppm and a very weak cross-peak to a signal at 2.76 ppm. The signal at 2.25 ppm has NOE cross-peaks to signals at 6.07 and 2.76 ppm. A strong 6.07−2.76 NOE cross-peak was also found. An NOE cross-peak was found to connect signals at 2.76 and 4.20 ppm. From these observations, the H1′, H2′, H2″, H3′, and H4′ signals were assigned (Table 1). The strong H8−H2′ NOE cross-peak suggests that this residue is anti,[55,57,58] and the observed H8−H3′ NOE cross-peak is consistent with an N-sugar pucker,[55] characteristic of the 5′-G* residue.[12,26−29,32,42,44] The 5′-G* H8 shift is relatively upfield, consistent with L canting of the 5′-G*.[27] This anti,anti HH conformer is assigned as HH1. In this and other cases, we differentiated between the two anti,anti HH conformers, HH1 and HH2, by utilizing characteristic key spectral features of the HH2 conformer. These features are downfield-shifted G* H8 signals with nearly similar shifts (shift separation normally less than 0.2 ppm), weak or absent H8-sugar NOE cross-peaks, and a very downfield-shifted ^{31}P NMR signal (ca. −1.8 ppm).[5,29,42,44] The similarity of the ^{31}P NMR resonance observed at −2.83 ppm (Figure 5) to chemical shifts observed for (*S,R,R,S*)-**Bip**Pt(d(G*pG*))[27] and other **L**Pt(d(G*pG*)) adducts confirmed the HH1 conformer assignment.[5,26,29]

For the less stable conformer (still abundant at 1 day), no H8−H8 NOE cross-peak was detected, indicating an HT arrangement of the G* bases.[5,27−29,42,44] The more downfield H8 signal (7.77 ppm) had a strong NOE cross-peak to a peak at 6.00 ppm, which showed NOE cross-peaks with signals at 2.65 and 3.31 ppm. The 6.00−2.65 ppm NOE cross-peak was stronger than the 6.00−3.31 ppm cross-peak. The 2.65 and 3.31 ppm signals were connected in the NOESY spectrum. The signal at 2.65 ppm had an NOE cross-peak to a signal at 4.12 ppm. The peak at 3.31 ppm also showed an NOE to a signal at 5.33 ppm. Thus, the H1′, H2′, H2″, H3′, and H4′ signals were assigned (Supporting Information). These signals are from the 3′-G* residue because the coupling of the assigned H1′ signal is consistent with an S-sugar pucker.[55,56] A strong H8−H1′ NOE and a downfield H2′ signal indicate a syn conformation.[27−29,42,44,55,57−60]

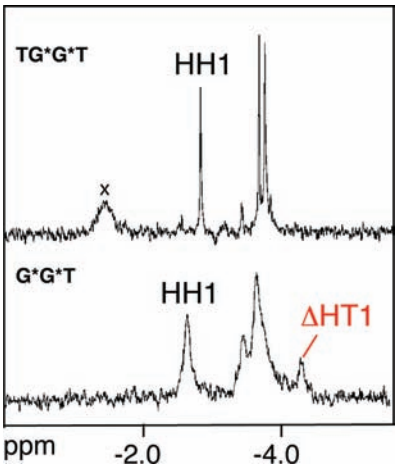

Figure 5. ^{31}P NMR spectra of (*S,R,R,S*)-**Bip**Pt(d(TG*G*T)) and (*S,R,R,S*)-**Bip**Pt(d(G*G*T)) adducts at pH 4.0 and 25 °C. The labels mark signals of the d(G*pG*) phosphate group. The signal labeled with X shifted ~1 ppm downfield as the pH was increased to ~7, indicating an impurity in the sample.

The more upfield H8 signal (7.69 ppm) showed NOE cross-peaks to signals at 2.64 and 3.67 ppm. These two signals were connected by an NOE cross-peak. The signal at 2.49 ppm also showed an NOE cross-peak to a signal at 2.64 ppm, which showed a cross-peak to a signal at 4.19 ppm. A signal at 6.23 ppm, assigned to H1′ from the distinctive shift, showed an NOE cross-peak to the signal at 2.64 ppm. From these observations, the H1′, H2′, H2″, H3′, and H4′ signals were assigned (Supporting Information). The intranucleotide H8−H2′/H2″ NOE cross-peaks and the very weak H8−H1′ NOE cross-peak suggest an anti conformation.[55,57,58] The strong H8−H3′ NOE cross-peak indicates an N-sugar pucker,[55,56] consistent with a 5′-G*.[12,26−29,32,42,44]

In a recent investigation of ^{13}C NMR shifts for the HH1 and ΔHT1 conformers of **Me$_4$DAB**Pt(d(G*pG*)) adducts (**Me$_4$DAB** = *N,N,N′,N′*-tetramethyl-2,3-diaminobutane, Figure 3),[42] we discovered characteristic C8 and C1′ NMR shifts for the ΔHT1 conformer. With the goal of evaluating the broad utility of this new information, we first assessed the effect of the carrier ligand on the structure of the macrocyclic ring by comparing ^{13}C NMR shifts of the HH1 and ΔHT1 conformers for the (*S,R,R,S*)-**Bip**Pt(d(G*pG*)) adduct with those for the **Me$_4$DAB**Pt(d(G*pG*)) adducts.[42] The ^{13}C NMR data for (*S,R,R,S*)-**Bip**Pt(d(G*pG*)) (Supporting Information) show the 5′-G* and 3′-G* C8 signals of the HH1 conformer at ~141 ppm, consistent with G platination at N7.[42,53] However, the 5′-G* and 3′-G* C8 shifts for the ΔHT1 conformer were at 140.6 and 145.7 ppm, respectively. Strikingly, these ^{13}C NMR shifts are very similar to those obtained for the ΔHT1 conformer in **Me$_4$DAB**Pt(d(G*pG*)) adducts,[42] suggesting an unusual positioning of the 3′-G* base and possibly the 5′-G* base of the ΔHT1 conformer. The HH1 5′-G* and 3′-G* C1′

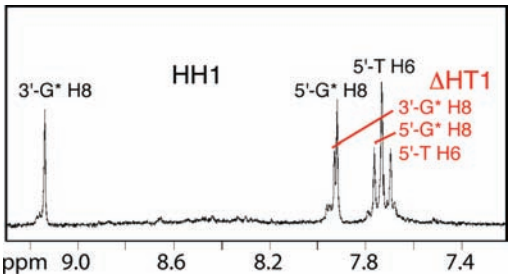

Figure 6. G* H8/T H6 region of the 1D NMR spectrum for (*S,R,R,S*)-**Bip**Pt(d(G*G*T)) at equilibrium (pH 4.0, 23 °C).

signals had normal shifts (~85 ppm),[42,53] whereas the ΔHT1 5′-G* and 3′-G* C1′ signals exhibited downfield shifts at ~86.1 and 89.1 ppm, respectively (Supporting Information).[14,53] C8 and C1′ signals are known to be more downfield in syn G* than in anti G* residues.[61,62] Furthermore, all C3′ sugar signals were observed at ~73−74 ppm, relatively upfield compared to that of an unplatinated G residue (79 ppm).[42,53] Consistent with previous studies,[14,42,53,61] the ~72−74 ppm shift for the 5′-G* residue is characteristic of an N-sugar pucker for the 5′-G* sugar (determined by NOESY and COSY data) while the C3′ upfield shift of the 3′-G* residues is typical for a 3′ terminal residue.[14,42,53,61] Taken together, the similarity of ^{13}C NMR shifts for (*S,R,R,S*)-**Bip**Pt(d(G*pG*)) and **Me$_4$DAB**Pt(d(G*pG*)) adducts[42] indicates that the carrier ligand has virtually no effect on the structure of HH1 and ΔHT1 conformers.

To determine the structural effect of residues flanking the G*G* lesion, we obtained ^{13}C NMR data for the (*S,R,R,S*)-**Bip**Pt(d(TG*G*T)) adduct. The HMQC NMR spectrum was collected when the HH1:ΔHT1 ratio was ~1:1. Overall, the G* C8 and C1′ NMR shifts for the HH1 and the ΔHT1 conformers are very similar to those observed for the respective conformers in the parent (*S,R,R,S*)-**Bip**Pt(d(G*pG*)) adduct (Supporting Information). Altogether, our data indicate that the similarity of the ^{13}C NMR shifts for (*S,R,R,S*)-**Bip**Pt(d(G*pG*)), (*S,R,R,S*)-**Bip**Pt(d(TG*G*T)), and **Me$_4$DAB**Pt(d(G*pG*))[42] adducts must be indicative of similar structural features of conformers. Of particular note, the new results confirm our past conclusion[42] that the unique structural features of the ΔHT1 conformer must be universal regardless of the nature of the carrier ligand. The new results extend this conclusion to cases in which flanking residues are present.

(*S,R,R,S*)-BipPt(d(TG*G*)). Three new pairs of G* H8 signals were observed ~20 min after initiation of the reaction. After 2 days, one downfield pair had disappeared, but the reaction forming the adduct was not complete until after 3 days. The 2D NMR data were all collected at this time (3−4 days), and the two abundant conformers were assigned to HH1 and ΔHT1, with a distribution of 70% and 30%, respectively (Supporting Information). With time, the ΔHT1 signals decreased in intensity; equilibrium was reached after 20 days, with a final HH1:ΔHT1 ratio of 97:3 (Figure 4). The ^{1}H−^{13}C HMQC spectrum for (*S,R,R,S*)-**Bip**Pt(d(TG*G*)) was collected when the HH1:ΔHT1 distribution was ~97:3. Thus, only the ^{13}C signals of the abundant HH1 conformer were assigned (Supporting Information). Interestingly, except for the C3′ upfield shift of the 3′-G* residue, which is typically more upfield for a terminal residue (~73 ppm), the ^{13}C NMR shifts are very similar to those obtained for the (*S,R,R,S*)-**Bip**Pt(d(TG*G*T)) adduct (Supporting Information), indicating that the 3′-T residue has no effect on the structure of the macrocyclic ring.

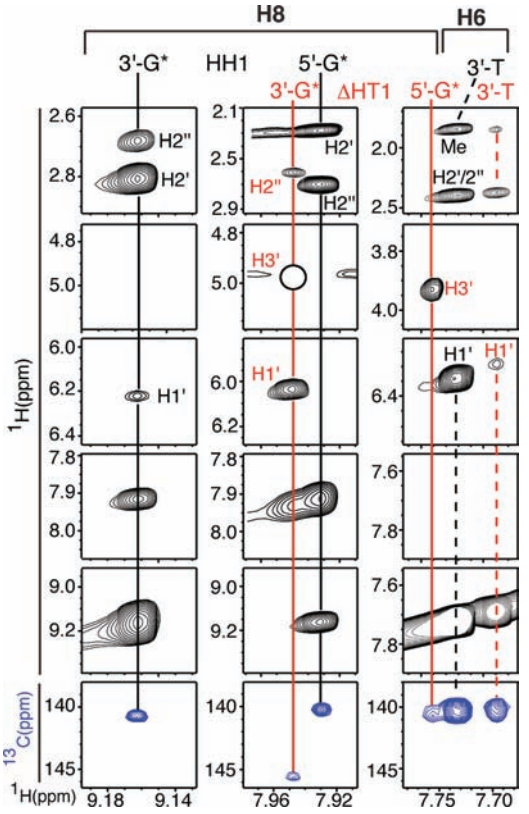

Figure 7. Selected regions of the 2D NOESY (black cross-peaks) and HMQC (blue cross-peaks) spectra obtained for (*S,R,R,S*)-**Bip**Pt(d(G*G*T)) at pH 4.0 (in 100% D_2O). The cross-peak marked with a circle overlaps with the HDO signal and thus is saturated.

(*S,R,R,S*)-BipPt(d(TTTG*G*)). Three new pairs of G* H8 signals were observed 1 h after the initiation of the reaction. One downfield pair of signals disappeared after 1 day. After 2 days, the reaction was complete (HH1:ΔHT1 ratio was 40:60). After equilibrium was reached (25 days), the HH1:ΔHT1 ratio was 97:3 (Figure S4 Supporting Information). The 5′-G* H8 signal of the HH1 conformer is broad but sharpens at higher temperature (Supporting Information), suggesting that dynamic motion of the 5′-TTT chain at low temperature borders on being a process that is slow on the NMR time scale.

(*S,R,R,S*)-BipPt(d(G*G*T)). Three new pairs of G* H8 signals were observed ~1 h after initiation of the reaction. After 2 days, the reaction was complete and one pair of G* H8 signals had disappeared. After 7 days, equilibrium was reached, with a final distribution of 65% and 35% for the two abundant conformers (Figure 6). From the 2D NOESY (Figure 7) and COSY data, the two abundant conformers are assigned to HH1 and ΔHT1. The d(G*pG*) ^{31}P NMR shifts confirm conformer assignment (Figure 5 and Table 1). As revealed by the 2D ^{1}H−^{13}C HMQC data (Figure 7), the ^{13}C NMR shifts (Supporting Information) are very similar to those obtained for (*S,R,R,S*)-**Bip**Pt(d(G*pG*)), (*S,R,R,S*)-**Bip**Pt(d(TG*G*T)), and (*S,R,R,S*)-**Bip**Pt(d(TG*G*)), indicating that the structure of the macrocyclic ring in the HH1 and ΔHT1 conformers is similar for these adducts regardless of the presence or position of the flanking residue.

dx.doi.org/10.1021/ic2011716 |*Inorg. Chem.* 2011, 50, 8608–8620

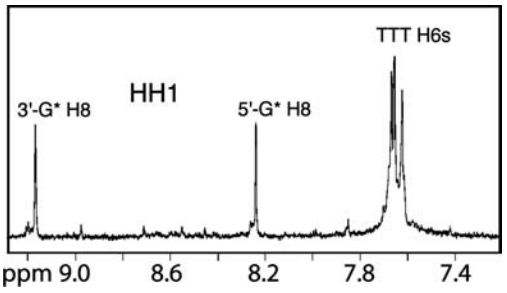

Figure 8. G* H8/T H6 region of the 1D NMR spectrum for (*S,R,R,S*)-**Bip**Pt(d(pG*G*TTT)) at equilibrium (23 °C). Labels mark the G* H8 signals of conformers.

(*S,R,R,S*)-BipPt(d(G*G*TTT)). Three new pairs of G* H8 signals were observed ~2 h after initiation of the reaction. The reaction was complete after 2 days (HH1:ΔHT1 = 30:70). The intensity of the ΔHT1 G* H8 signals decreased with time, and equilibrium was reached in 14 days (HH1:ΔHT1 65:35). Interestingly, in contrast to what was observed for the (*S,R,R,S*)-**Bip**Pt(d(TTTG*G*)) adduct, neither of the G* H8 signals was broad at room temperature. We cannot rule out that the 3′-TTT chain, which can possibly undergo some dynamic motion that is slow on the NMR scale, is too far from the G* H8 atoms to have any effect on line width. However, we believe that the absence of an effect of the 3′-TTT side chain and the broadening effect of the 5′-TTT side chain are consistent with the close proximity of the latter to the carrier ligand.

(*S,R,R,S*)-BipPt(d(pG*G*TTT)). Three new pairs of G* H8 signals were observed ~15 min after initiation of the reaction. Reaction was complete after 1 day. After 2 days, the unstable conformer had disappeared and the HH1:ΔHT1 ratio was ~1:1. The ΔHT1 signals decreased with time, becoming barely visible after 20 days (final HH1:ΔHT1 ratio = 94:6, Figure 8). The d(G*pG*) ^{31}P NMR signals at −2.98 and −4.08 ppm are assigned to the HH1 and ΔHT1 conformers, respectively. As the pH was increased from 4.0 to 7.6, the ^{31}P NMR signal at −2.54 ppm became broad and shifted downfield by ~1.2 ppm; this signal was assigned to the 5′-p group. No shift occurred for the ^{31}P signals at −2.98 and −4.08 ppm. Likewise, the G* H8 signals did not exhibit chemical shift changes when the pH was raised from 4.0 to 7.6. This result is very different from that observed previously for the (*R,S,S,R*)-**Bip**Pt(d(pG*G*TTT)) adduct[19] (a detailed analysis of the dependence of H bonding on pH is presented below).

(*S,R,R,S*)-BipPt(d(HxapG*G*T)). Three new pairs of G* H8 signals were observed ~15 min after initiation of the reaction. After ~1 day, the reaction was complete. After ~2 days, the two remaining pairs were assigned to the HH1 (~67%) and ΔHT1 (~33%) conformers. The intensity of the ΔHT1 G* H8 signals decreased with time, and the signals became barely visible after 14 days (Supporting Information). The final HH1:ΔHT1 ratio was 95:5. Four ^{31}P NMR signals were observed outside the normal shift range (from ca.−3.7 to −3.9 ppm).[47] Because they have shifts similar to that of the Hxap group in free d(HxapGGT),[19] the ^{31}P NMR signals at −2.35 and −2.55 ppm were assigned to the Hxap group. From their relative intensity, they were, respectively, assigned to the HH1 and ΔHT1 conformers. The ^{31}P NMR signals observed at −3.11 and −4.22 ppm are assigned to d(G*pG*) of the HH1 and ΔHT1 conformers, respectively, because of the similarity in chemical shifts to those observed previously for the (*S,R,R,S*)-**Bip**Pt(d(G*pG*)) adduct.[27]

DISCUSSION

Our previous results on **Me$_2$ppz**Pt(oligo) and (*R,S,S,R*)-**Bip**Pt(oligo) adducts revealed the value of studying **L**Pt(oligo) ss models in explaining the differences in features between ss and duplex adducts.[19,20] Treatment of DNA duplexes can produce ss structures such as coils and hairpins.[4,61,63]

In our **Me$_2$ppz**Pt(oligo)[20] and (*R,S,S,R*)-**Bip**Pt(oligo)[19] studies, we focused mainly on the HH1 conformer. The degree of G* base canting ranged from minimal for the **Me$_2$ppz**Pt(oligo) adducts to distinct R canting for the (*R,S,S,R*)-**Bip**Pt(oligo) adducts. The very L-canted (*S,R,R,S*)-**Bip**Pt(oligo) models in this study reveal several new features of **L**Pt(oligo) ss complexes, allowing us to assess the effect of flanking residues on conformer distribution, G* base canting, and backbone geometry and the relevance of hydrogen bonding. At the end of this discussion, we use our studies of less dynamic models to re-evaluate some NMR characteristics of previously studied dynamic **L**Pt(oligo) ss adducts, such as the **en**Pt(d(TG*G*T))[47] adduct (**en** = ethylenediamine).

These assessments were made possible by our ability to detect multiple conformers of the (*S,R,R,S*)-**Bip**Pt(oligo) adducts investigated here by NMR spectroscopy. By applying our standard assignment protocols (e.g., NOE data, ^{1}H−^{1}H coupling, and ^{31}P data), we could assign the HH1 and ΔHT1 conformation to all abundant conformers observed for all (*S,R,R,S*)-**Bip**Pt(oligo) adducts (Supporting Information). Because previous **L**Pt(oligo) studies employed dynamic adducts,[45−47] such an in-depth study was not possible.

Base Canting. The two most significant structural parameters involving the bases are HH or HT orientation and base canting (Figure 1). In most adducts, which usually have relatively small carrier ligands, the bases do not lie exactly perpendicular to the coordination plane. The degree and direction (L or R) of canting (Figure 1) depend on the carrier ligand, on the presence or absence of a linkage between the bases, on the presence or absence of a flanking residue, and even on the ss or duplex character of the DNA. As suggested previously,[44] the degree and direction of canting help to define the cisplatin-induced distortion in DNA. Thus, canting is an important structural component expected to influence biological activity.

For adducts with two cis guanines, the H8 shifts reflect the positional relationship of the H8 of one guanine to the ring current of the cis guanine. Normally, differences in canting influence the position and, hence, shift. Recently, we introduced a new structural explanation for the H8 shifts specific to the ΔHT1 conformer (see below).[42,44] However, the well-accepted canting explanation works well in the typical cases.[19,24,26,27] Typically, H8 signals for clearly canted and less canted bases of HH conformers have chemical shifts of ~7.8−8.3 and ~8.7−9.2 ppm, respectively.[26,27] The H8 of a canted G* base experiences the shielding effect of the anisotropic cis G* base.[24] The H8 of a less canted base is positioned away from the cis G* base and is deshielded by the Pt inductive effect and possibly magnetic anisotropy.[29,64−66] However, other factors also come into play. In Pt(d(G*pG*)) adducts, a ca. 0.3 ppm downfield shift of the 3′-G* H8 atom is caused by the 3′-G* 5′-phosphate group.[19,26] For an HH1 conformer, such NMR data suggest for uncanted G* bases H8 shifts of 8.8 (5′-G*) and 9.2 ppm (3′-G*) and for canted

Figure 9. Comparison of 5′-G* and 3′-G* H8 shifts of the HH1 conformer for all (*S,R,R,S*)-**Bip**Pt(oligo) adducts at 5 °C and pH ≈ 4. The G* H8 shifts for the (*S,R,R,S*)-**Bip**Pt(d(G*pG*)) adduct (5 °C and pH ≈ 4) were reported previously.[27]

G* bases H8 shifts of 7.9 (5′-G*) and 8.2 ppm (3′-G*). For example, the two G* H8 signals differ by ∼1.2 ppm for the HH1 conformer of the (*S,R,R,S*)-**Bip**Pt(d(G*pG*)) adduct, which is left-handed, with a clearly canted 5′-G* base (shift ∼8 ppm) and a less canted 3′-G* base (shift ≈ 9.2 ppm).[26−28] Minor shift variations (0.1−0.2 ppm) observed for H8 signals of the HH1 conformer as the carrier ligand changes can be attributed to secondary factors, such as carrier-ligand influence on the inductive effect of the Pt(II) center.[5,44]

Comparison of the G* H8 shifts of the (*S,R,R,S*)-**Bip**Pt(oligo) adducts to those of the parent (*S,R,R,S*)-**Bip**Pt(d(G*pG*)) adduct (Table 1 and Figure 9) is the standard approach for assessing the influence of the flanking residue type (phosphate group or complete T residue) or the length of the flanking nucleotide chain (T or TTT) on base canting of the HH1 conformer. We must factor out the relative contribution of through-space anisotropic effects of flanking residues on the G* H8 shifts. The anisotropic effect of a phosphate group can deshield the closest atoms (e.g., H8 atom). The presence of a flanking 5′-p group was found to cause a significant downfield shift of the 5′-G* H8 signal.[23,47,67] The anisotropy of the T nucleobase can shield the H8 atom. A flanking T nucleotide residue thus has both deshielding and shielding moieties.

Flanking 3′-groups have been shown to be too far from the 3′-G* H8 to have much direct influence on the H8 shift.[19,20] In the following, we first show that 3′-flanking residues have no effect on the NMR shifts or structures of (*S,R,R,S*)-**Bip**Pt(oligo) adducts. Next, we discuss how the G* H8 shifts and other properties of the HH1 conformer of (*S,R,R,S*)-**Bip**Pt(oligo) adducts depend on the 5′-flanking T residues in the absence of a 3′-flanking T residue. Finally, we assess adducts with 3′-T residues and 5′-flanking substituents.

Influence of Only 3′-T Residues on G* Base Canting. The HH1 conformer of the (*S,R,R,S*)-**Bip**Pt(oligo) complexes with one or more 3′-flanking T residues has 5′- and 3′-G* H8 shifts that are very similar to the respective shifts of (*S,R,R,S*)-**Bip**Pt(d(G*pG*)) (Table 1 and Figure 9). This result establishes that the 3′-flanking residue does not influence the degree of G* base L canting for the Ptd(G*pG*) moiety, consistent with the findings on the **Me$_2$ppz**Pt(d(G*G*T)) and (*R,S,S,R*)-**Bip**Pt(oligo) adducts.[19,20]

Influence of Only 5′-T Residues on G* Base Canting. For the (*S,R,R,S*)-**Bip**Pt(d(TG*G*)) and (*S,R,R,S*)-**Bip**Pt(d(TTTG*G*)) complexes, the 3′-G* H8 shifts are only slightly downfield from the 3′-G* H8 signal of the (*S,R,R,S*)-**Bip**Pt(d(G*pG*) adduct; however, the 5′-G* H8 shifts are moderately downfield (from ∼0.20 to 0.26 ppm, Table 1 and Figure 9). The minor nature of these changes indicates that the changes in canting caused by the 5′-substituents are not significant and are probably negligible. (*S,R,R,S*)-**Bip**Pt(oligo) complexes are very L canted. Thus, the moderate downfield shift of the 5′-G* H8 signal for the (*S,R,R,S*)-**Bip**Pt(d(TG*G*)) and (*S,R,R,S*)-**Bip**Pt(d(TTTG*G*)) complexes is caused by either the steric bulk of the 5′-flanking residue or the anisotropic effect of this residue. The anisotropic effect of the 5′-T residue reflects a combination of the deshielding phosphate effect and the anisotropic shielding effect of the base. These two effects cancel for the HH1 conformer of (*R,S,S,R*)-**Bip**Pt(oligo) adducts.[19] Thus, the moderate nature of the 5′-G* H8 downfield shift (from ∼0.2 to 0.26 ppm) for the (*S,R,R,S*)-**Bip**Pt(d(TG*G*)) and (*S,R,R,S*)-**Bip**Pt(d(TTTG*G*)) adducts most likely is caused by the effect of steric bulk on canting. The anisotropic effect of the 5′-substituent will be considered in more detail below.

Combined Influence of 5′- and 3′-Substituents. *d(TG*G*T) Adduct.* For (*S,R,R,S*)-**Bip**Pt(d(TG*G*T)), the G* H8 shifts are very similar to those of the (*S,R,R,S*)-**Bip**Pt(d(TG*G*)) complex (Table 1 and Figure 9). This result extends to adducts that possess a 5′-substituent the finding that a 3′-substituent has no influence on (*S,R,R,S*)-**Bip**Pt(oligo) adducts. The 5′-substituent clearly is more important than the 3′-substituent in influencing base canting and H8 shifts of the cross-link moiety.

*d(pG*G*TTT) Adduct.* In investigations of the effect of the 5′-p group on canting for the R-canted (*R,S,S,R*)-**Bip**Pt(d(pG*G*TTT)) complex[19] and for the minimally canted **Me$_2$ppz**Pt(d(pG*pG*)) adduct,[20] we found that the influence on canting of the 5′-p group is smaller than that of a complete 5′-T residue. Another important observation for the HH1 conformer of the (*R,S,S,R*)-**Bip**Pt(d(pG*G*TTT)) adduct was the strong evidence for hydrogen bonding between the 5′-p group and the **Bip**(NH) group.[19] Because the positions of the **Bip**(NH) groups differ for the *S,R,R,S* and *R,S,S,R* isomers, it is not possible for the 5′-p group to form an H bond with the cis NH group in the HH1 conformer of the (*S,R,R,S*)-**Bip**Pt(d(pG*G*TTT)) complex. Thus, a comparison of **Bip**Pt(d(pG*G*TTT) adducts, as permitted by the present investigation, is particularly informative for analyzing the effect of hydrogen bonding on canting and structure.

For (*S,R,R,S*)-**Bip**Pt(d(pG*G*TTT)), the 5′-G* H8 signal is 0.37 ppm more downfield than the 5′-G* H8 signal of the (*S,R,R,S*)-**Bip**Pt(d(G*pG*)) adduct; however, this signal is only 0.1 ppm more downfield than the 5′-G* H8 signal for the (*S,R,R,S*)-**Bip**Pt(d(TG*G*)) and (*S,R,R,S*)-**Bip**Pt(d(TG*G*T)) complexes. As the pH was raised from ∼4 to ∼7, the 5′- and 3′-G* H8 signals of the HH1 conformer did not shift (Figure 9). In contrast, for (*R,S,S,R*)-**Bip**Pt(d(pG*G*TTT)),[19] the 5′-G* H8 signal was significantly more downfield (0.28 ppm) than for the (*R,S,S,R*)-**Bip**Pt(d(TG*G*T)) complex, and this H8 signal shifted 0.27 ppm downfield when the pH was increased from ∼4 to ∼7. This observation for (*R,S,S,R*)-**Bip**Pt(d(pG*G*TTT)) supports a 5′-p−**Bip**(NH) interaction that positions the 5′-p close to the 5′-G* H8 atom, suggesting that the downfield shift for the 5′-G* H8

dx.doi.org/10.1021/ic2011716 |*Inorg. Chem.* 2011, 50, 8608–8620

Table 2. Equilibrium Distribution for (*S,R,R,S*)-BipPt(oligo) Adducts (pH ≈ 4)

adduct	% HH1	% ΔHT1
d(G*pG*)[a]	65	35
d(G*G*T)	65	35
d(G*G*TTT)	68	32
d(TG*G*)	97	3
d(TTTG*G*)	97	3
d(TG*G*T)	96	4
d(pG*G*TTT)	94	6
d(HxapG*G*T)	95	5

[a] Reference 27.

signal upon deprotonation is caused by increased phosphate group anisotropy and stronger H bonding. The absence of any corresponding pH-dependent downfield shift of the 5′-G* H8 signal for (*S,R,R,S*)-**Bip**Pt(d(pG*G*TTT)) indicates that the 5′-p group is not close enough to the H8 atom to have a large deshielding effect on the H8 signal.

*d(HxapG*G*T) Adduct.* In order to understand more about the effect of the 5′-phosphodiester group size on canting, we studied the (*S,R,R,S*)-**Bip**Pt(d(HxapG*G*T)) complex. The 5′-G* H8 shift for this adduct is intermediate between the 5′-G* H8 shifts of the (*S,R,R,S*)-**Bip**Pt(d(TG*G*T)) and (*S,R,R,S*)-**Bip**Pt(d(pG*G*TTT)) complexes (Figure 9). In addition to the phosphate effect of the Hxap group on the 5′-G* H8 signal, the steric bulk also plays a role in altering canting to a small degree. Because the 5′-G* H8 signal for the (*S,R,R,S*)-**Bip**Pt(d(HxapG*G*T)) complex is only slightly different from that for the (*S,R,R,S*)-**Bip**Pt(d(TG*G*T)) or (*S,R,R,S*)-**Bip**Pt(d(TG*G*)) complexes, we conclude that the effect of the Hxap group on canting is small but essentially similar to that of the 5′-T residue. These groups were also found to have a similar effect in (*R,S,S,R*)-**Bip**Pt(oligo) adducts.[19]

Summary. L canting for the (*S,R,R,S*)-**Bip**Pt(oligo) adducts decreases slightly over the series d(G*pG*) ≈ d(G*G*T) ≈ d(G*G*TTT) > d(TTTG*G*) > d(TG*G*T) ≈ d(TG*G*) ≈ d(HxapG*G*T) > d(pG*G*TTT). Note that in comparison to the (*R,S,S,R*)-**Bip**Pt(oligo) and **Me$_2$ppz**Pt(oligo) adducts,[19,20] (*S,R,R,S*)-**Bip**Pt(oligo) adducts lacking a 5′-substituent are *more* canted. Thus, although the steric effects of the 5′-substituent in (*S,R,R,S*)-**Bip**Pt(oligo) adducts decrease the L canting by a small degree, L canting is still rather large for all adducts.

Conformer Distributions. In Table 2, the conformer distributions of (*S,R,R,S*)-**Bip**Pt(oligo) and (*S,R,R,S*)-**Bip**Pt(d(G*pG*)) adducts are compared. The conformer distributions of (*S,R,R,S*)-**Bip**Pt(d(G*G*T)) and (*S,R,R,S*)-**Bip**Pt(d(G*G*TTT)) complexes, even after many days, are similar to that of the (*S,R,R,S*)-**Bip**Pt(d(G*pG*)) complex, indicating that the 3′-flanking residue is too remote from both the carrier ligand and the 5′-G* residue to influence conformer distribution for (*S,R,R,S*)-**Bip**Pt(oligo) adducts. The ΔHT1 conformer is about one-half as abundant as the HH1 conformer at equilibrium for (*S,R,R,S*)-**Bip**Pt(oligo) complexes with only 3′-substituents. Thus, the ΔHT1 conformation of the macrocycle is about 0.4 kcal mol^{-1} less favorable than the HH1 conformation.

In contrast, although the ΔHT1 conformer for (*S,R,R,S*)-**Bip**Pt(oligo) complexes with 5′-substituents formed as a kinetic product, the ΔHT1 conformer disappeared almost completely within ∼14−25 days as the HH1 conformer became abundant. Thus, the HH1 conformer is highly favored over the ΔHT1 conformer. Likewise, the ΔHT1 conformer for **Me$_2$ppz**Pt(oligo) adducts with a 5′-substituent formed as a kinetic product, but this conformer also disappeared almost completely after many days.[20] Evidence for the high stability of the HH1 conformer for adducts with a 5′-flanking residue was also obtained for (*R,S,S,R*)-**Bip**Pt(oligo) adducts, for which no ΔHT1 conformer was found.[19] The combined results for these **L**Pt(oligo) complexes establish that the additional lower stability of the ΔHT1 conformer (and hence additional higher stability of the HH1 conformer) occurs only when the residue flanking the d(G*pG*) cross-link lesion is in the 5′ position. Thus, the ΔHT1 conformation of the macrocycle is ∼3 kcal mol^{-1} less favorable than the HH1 conformation when there is a 5′-substituent.

A minimized model of the ΔHT1 model of (*S,R,R,S*)-**Bip**Pt(d(G*pG*)) shows that the 5′-OH group points toward the six-membered ring of the 3′-G* residue.[27] A 5′-substituent is very likely to clash with the 3′-G* residue, explaining why the ΔHT1 conformer, a kinetic product formed in high abundance in some cases, is thermodynamically disfavored when a 5′-substituent is present. Consistent with this model, the ΔHT1 conformer is unstable in adducts having moderately bulky carrier ligands differing in chirality and potential for hydrogen bonding.[19,20] Thus, for these cases, it is reasonable to conclude that the lower stability of the ΔHT1 conformer can be attributed to steric clashes of the 5′-substituent with the 3′-G* residue and not with the carrier ligand. The present results establish that this situation is affected little by canting direction.

Effect of Flanking Substituents on Initial Formation of Reaction Products. Soon after addition of the [(*S,R,R,S*)-**Bip**Pt(NO$_3$)$_2$] solution to oligos with only 3′-substituents, two downfield, equal-intensity H8 signals (∼8.7−9.0 ppm) were observed (Supporting Information). The intensity of this pair of signals was twice that of either the HH1 or the ΔHT1 pair of H8 signals. Despite the initial large intensity, the pair of signals disappeared after ∼1−2 days. These two signals were too short lived to allow a detailed study, but the initially formed abundant unstable intermediate is undoubtedly from a third conformer. We believe that this third conformer most likely is the now well-established HH2 conformer frequently observed with a number of carrier ligands.[5,26,29,42,44] For the previously studied (*S,R,R,S*)-**Bip**Pt(d(G*pG*)) adduct, two downfield signals of equal intensity (at 8.68 and 8.73 ppm), thought to be of a third conformer, were also observed.[27] Similarly, for (*S,R,R,S*)-**Bip**Pt(d(G*G*T)) we observed two new signals at shifts almost identical to those of the respective d(G*pG*) complex (Supporting Information). An appreciable amount of the HH2 conformer was also observed for **Me$_2$ppz**Pt(d(G*pG*)),[29] (*R,R*)-**Me$_4$DAB**Pt(d(G*pG*)),[19] and other adducts.[5,44] Because the G* H8 shifts of these HH2 conformers for (*S,R,R,S*)-**Bip**Pt(oligo) complexes with a 3′-substituent are observed at 8.7−8.9 ppm, values very similar to those of the HH2 conformer of **Me$_2$ppz**Pt((dG*pG*)) and (*R,R*)-**Me$_4$DAB**Pt(d(G*pG*)), we conclude that the G* bases of the HH2 conformer of (*S,R,R,S*)-**Bip**Pt(d(G*G*T)) are not canted.

The decrease in abundance of the initially formed intermediate, very likely the HH2 conformer, and the parallel increase in that of the ΔHT1 conformer indicate that the putative HH2 conformer redistributes to the ΔHT1 conformer. Within 2 days, the relative HH1:ΔHT1 ratio was ∼40:60. Because at equilibrium the ΔHT1 conformer exists at a very low abundance (Table 2), the increase in its abundance as the HH2 conformer

decreases leaves no doubt that the HH2 conformer converts to the ΔHT1 conformer.

As shown in Figure 1, because sequential rotation of two bases is required, conversion of the HH2 to the HH1 conformer must pass through either the ΔHT1 or the ΛHT2 conformer. However, the ΛHT2 conformer is not stable and thus is unlikely to be the intermediate. The present results provide direct evidence that the HH2 conformer forms the ΔHT1 conformer.

Compared to the reactions of oligos having only a 3′-flanking residue, in early stages of the reaction forming the (*S,R,R,S*)-**Bip**Pt(oligo) adducts with a 5′-substituent, the ΔHT1 conformer formed in lower abundance (40−50% vs 60%) (Supporting Information). Also, oligos having a 5′-substituent formed the third conformer (probably HH2) in much lower abundance; again, this third conformer disappeared in ∼1−2 days. After ∼20 days, the ΔHT1 conformer abundance had become very low (from ∼3% to 6%). The lower abundance of the HH2 and ΔHT1 conformers makes the interpretation of results with oligos having a 5′-substituent less compelling than the clear interpretation of the results with oligos having only a 3′-substituent. Nevertheless, the spectra (Supporting Information) are consistent with a kinetically favored HH2 conformer (formed during addition reaction of the oligo) isomerizing to a kinetically favored ΔHT1 conformer, which in turn isomerizes somewhat slowly to the thermodynamically favored HH1 conformer.

Comparison between ss and Duplex Adducts. As evident from our data on the (*S,R,R,S*)-**Bip**Pt(oligo) adducts, the shifts and couplings of the G*G* sugar signals of the HH1 conformer are very similar (Table 1). This similarity leads us to conclude that although the 5′-substituent has some moderate influence on base canting, it causes no detectable changes in backbone geometry, consistent with the X-ray data[11,25] and our findings for the (*R,S,S,R*)-**Bip**Pt(oligo)[19] and **Me$_2$ppz**Pt(oligo)[20] adducts.

The sugar moieties of the 5′- and 3′-G* residues of significant (*S,R,R,S*)-**Bip**Pt(oligo) conformers were found to have the N- and S-pucker conformations, respectively. Adoption of the N-sugar pucker conformation by the 5′-G* is a universal property of **L**Pt cross-link adducts.[5,14,20,22,26,27,29,42,44,53,54] In comparison, the 3′-G* sugar in these **L**Pt adducts retains the S-pucker conformation favored by B-DNA.

As indicated by the NOE data and $J_{H1'-H2'}/J_{H1'-H2''}$ values for the T residues for the (*S,R,R,S*)-**Bip**Pt(oligo) adducts (Supporting Information), the S pucker is clearly retained for the HH1 conformer. These results are in good agreement with recent findings for the (*R,S,S,R*)-**Bip**Pt(oligo)[19] and **Me$_2$ppz**Pt(oligo) adducts[20] and with previous X-ray[25] and NMR[45−47] data on *cis*-Pt(NH$_3$)$_2$(oligo) adducts, showing that the sugar of the X residue in the XG*G* lesion retains the S pucker.

Indeed, the (*S,R,R,S*)-**Bip**Pt(oligo) complexes do not exhibit the characteristic spectral and structural features observed for the XG* step in duplex models[14] (a large upfield X H2′ shift as a result of the anisotropy effect of the 5′-G* base and an N pucker for the X residue). We recently interpreted these features in duplexes as arising from the position that the 5′-X residue must adopt in order to form a WC base pair.[19,20] This position in turn leads to the large positive shift and slide that make the XG* bp step so distinctive. The position also dictates that the canting is R. Thus, the new results for the L-canted (*S,R,R,S*)-**Bip**Pt(oligo) adducts and those for the previously studied **Me$_2$ppz**Pt(oligo)[20] and (*R,S,S,R*)-**Bip**Pt(oligo) adducts[19] indicate that the S-to N-pucker change of the 5′-X residue in duplexes is not dependent on canting, but the change in X-residue sugar pucker in duplexes is needed to move the X residue to a position that permits formation of X·X′ WC H bonds. The change from L canting in ss to R canting in duplexes is needed to avoid severe clashes between the 5′-X and the 5′-G* residues when the 5′-X residue adopts the new position.

Comparison of Less Dynamic Adducts to Cisplatin−DNA Adducts. Two ideas concerning the cisplatin−DNA adduct have gained wide acceptance: (a) only one conformer (HH1) exists for the cisplatin-1,2 d(G*pG*) cross-link[23,24,32,46,52] and (b) the phosphodiester linkage hinders Pt−G* N7 bond rotation.[52] Over the past decade, these thoughts have been challenged and re-evaluated.[5,26−29,42,44] The fact that multiple conformers are present for **L**Pt(d(G*pG*))-type complexes suggests that such conformers may be present in the *cis*-Pt(NH$_3$)$_2$(d(G*pG*)) model complex. A mixture of rapidly interconverting conformers may account more fully for several spectral features and characteristics of the *cis*-Pt(NH$_3$)$_2$(d(G*pG*)) complex, including the following:[28] (a) the broadening of H8 NMR signals at lower temperature, (b) the chemical shift of the ^{31}P NMR signal, and (c) the difficulty in obtaining any crystallographic information.

Our studies with **Bip**Pt(oligo) complexes encouraged us to re-evaluate some of the spectral interpretations previously offered for platinated oligos. We focus mainly on *cis*-Pt(NH$_3$)$_2$ and **en**Pt ss models. In addition to ^{1}H and ^{13}C NMR data (discussed below), ^{31}P NMR shifts are also distinctive and characteristic of the multiple different conformers. A downfield-shifted ^{31}P NMR signal for the d(G*pG*) cross-linked moiety, relative to the free d(GpG), is a common spectral feature of the intrastrand lesion of platinated oligos.[14,26,32,47,68] However, through our studies of nondynamic adducts, we have now established that the d(G*pG*) ^{31}P NMR signal of the ΔHT1 conformer is shifted upfield (ranging in shift from ∼−4.0 to ∼−5.0 ppm but typically more upfield than ∼−4.5 ppm).[5,20,27−29,42,44] Investigations of **L**Pt(oligo) ss adducts that preceded these discoveries typically employed small NH-bearing carrier ligands; the finding of some slightly less downfield-shifted ^{31}P NMR signals of a few **L**Pt(oligo) adducts was explained by H-bonding interactions between the NH groups and the flanking residues.[47,68,69] This explanation was based on differences found between model complexes in which these H bonds are possible, compared to those in which such interactions are not (e.g., the presence or absence of carrier-ligand NH groups or 5′-flanking substituent).[47]

Before discussing these few unusual dynamic **L**Pt(oligo) adducts,[47] we shall compare the ^{31}P NMR shifts of the more typical dynamic **L**Pt(oligo) adducts with ^{31}P NMR shifts for the HH1 conformer of the (*S,R,R,S*)-**Bip**Pt(oligo) and the minimally canted **Me$_2$ppz**Pt(oligo) adducts.[70] The ^{31}P NMR shifts for the d(G*pG*) cross-link moiety for L-canted *cis*-Pt(NH$_3$)$_2$(d(TG*G*T)) and **en**Pt(d(TG*G*T))[47] adducts are −3.02 and −2.88 ppm, respectively. The ^{31}P NMR shift of the HH1 conformer was observed at −2.83 ppm for (*S,R,R,S*)-**Bip**Pt(d(TG*G*T)) and at −3.05 ppm for **Me$_2$ppz**Pt(d(TG*G*T)).[70] Three important points have emerged from these striking similarities in ^{31}P NMR shifts. First, the HH1 conformer is the most likely highly dominant conformer for the *cis*-Pt(NH$_3$)$_2$(d(TG*G*T)) and **en**Pt(d(TG*G*T)) complexes because this conformer dominates in the **Bip**Pt and **Me$_2$ppz**Pt complexes. Second, **L** H bonding is not a factor influencing such a ^{31}P NMR downfield shift because **Me$_2$ppz** lacks NH groups. Third, when **L**

has moderate (e.g., **Me$_2$ppz**) or small (e.g., $(NH_3)_2$) bulk, the ΔHT1 conformer is highly disfavored by a 5′-substituent.

The ^{31}P NMR shift of dynamic adducts reflects the dominant conformer in solution, but it can have components of minor conformers. If a dynamic adduct has a 2:1 ratio of HH1:ΔHT1 conformers and if the ^{31}P shifts are −3.0 (HH1) and −4.5 ppm (ΔHT1), a shift of ∼−3.5 ppm is expected. Indeed, the d(G*pG*) ^{31}P shift (−3.60 ppm)[47] for **en**Pt(d(G*G*TT)) is close to this value and significantly more upfield than any of the ^{31}P NMR signals for dynamic adducts mentioned above. Because we established that multiple conformers are present for **Bip**Pt(oligo) and **Me$_2$ppz**Pt(oligo) adducts with 3′-substituents,[19,20] we believe that the more upfield ^{31}P NMR signal of **en**Pt(d(G*G*TT)) very probably reflects the presence of a considerable abundance of the ΔHT1 conformer.

Further comparison between less dynamic adducts with the dynamic cisplatin−DNA adducts can be made by using the ^{13}C NMR shifts for these adducts (^{13}C NMR shifts are reported in the Supporting Information). We shall compare these shifts for (*S,R,R,S*)-**Bip**Pt(d(TG*G*T)) with the data reported for **en**Pt(d(TG*G*T)).[53] (As concluded above, the only conformer of **en**Pt(d(TG*G*T)) with any significant abundance is the HH1 conformer.) We observed previously that the HH1 and ΔHT1 conformers differ significantly in their C8 and C1′ shifts.[42] For (*S,R,R,S*)-**Bip**Pt(d(TG*G*T)), the HH1 5′-G* and 3′-G* C8 shifts were observed at 141.0 and 140.9 ppm, respectively; the corresponding ΔHT1 C8 shifts were at 140.6 and 145.7 ppm. The HH1 5′-G* and 3′-G* C1′ shifts were at 85.0 and 85.2 ppm and at 86.1 and 89.1 ppm for the ΔHT1 conformer, respectively. In comparison, for **en**Pt(d(TG*G*T)) the 5′-G* and 3′-G* C8 shifts were observed at 140.2 and 141.0 ppm, respectively, whereas the corresponding C1′ shifts were at 84.6 and 84.9 ppm.[53] Because the C8 and C1′ shifts for the (*S,R,R,S*)-**Bip**Pt(d(TG*G*T)) HH1 conformer are very similar to those reported for the **en**Pt(d(TG*G*T)) adduct,[53] the ^{13}C NMR shifts strongly support our conclusion that the latter compound exists in solution mainly as the HH1 conformer.

On the basis of the above analysis, we can draw the following conclusions: (a) The HH1 downfield-shifted ^{31}P NMR signals found for (*S,R,R,S*)-**Bip**Pt(oligo) complexes (Table 1) are comparable to those reported for adducts in which carrier-ligand NH-5′-p group H bonds do not exist.[20] This similarity indicates that NH-5′-p H bonding has little influence on the macrocylic ring conformation and, hence, on the chemical shifts of these ^{31}P NMR signals. (b) The downfield ^{31}P NMR signals for model adducts in fast dynamic conformer interchange (e.g., cisplatin and **en**Pt) represent mainly an HH1 conformer when a 5′-flanking residue is present; however, the more upfield ^{31}P NMR shifts of model adducts with no 5′-flanking residue indicate a mixture of rapidly interchanging HH and HT conformers with perhaps other minor conformers.

Another interesting point related to cisplatin−DNA model adducts has emerged from these (*S,R,R,S*)-**Bip**Pt(oligo) studies and the previous studies with **Me$_2$ppz**Pt(oligo)[20] and (*R,S,S,R*)-**Bip**(oligo) adducts.[19] Despite much effort, crystallographic data have never been obtained for the *cis*-Pt$(NH_3)_2$(d(G*pG*)) model adduct. However, the crystal structures of the *cis*-Pt$(NH_3)_2$(d(pG*pG*))[11,12] and *cis*-Pt$(NH_3)_2$(d(CG*G*))[25] complexes have been reported. The presence of the HH1 conformer almost exclusively for the **Bip**Pt(oligo) adducts with a 5′-flanking residue most probably is relevant to the analogous model complexes with cisplatin. The *cis*-Pt$(NH_3)_2$(d(G*pG*)) adduct exists as a mixture of conformers, making crystallization difficult. In contrast, the *cis*-Pt$(NH_3)_2$(d(pG*pG*)) and *cis*-Pt$(NH_3)_2$(d(CG*G*)) adducts both exist as a single dominant HH1 conformer, a circumstance facilitating crystallization.

CONCLUSIONS

This is the first report of NMR data on a nondynamic, very strongly L-canted model for *cis*-Pt$(NH_3)_2$(oligo) ss adducts. The 5′-substituent decreases L canting of the HH1 conformer of (*S,R,R,S*)-**Bip**Pt(oligo) adducts but by only a *small* degree. We conclude that weak steric clashes of the 5′-substituent with the carrier ligand are responsible for this *small* decrease. This result is in contrast with our previous study of the R-canted (*R,S,S,R*)-**Bip**Pt(oligo) adducts, in which the flanking 5′-substituent causes a relatively large decrease in canting.[19]

For all (*S,R,R,S*)-**Bip**Pt(oligo) adducts, the **Bip**(NH) cis to the 5′-substituent is located on the opposite side of the coordination plane as the 5′-p or XpG* phosphate group; thus, an H-bonding interaction between the NH, the 5′-p, or the XpG* phosphate group is not possible. This result is in agreement with the hypothesis that H bonding to such a flanking substituent is not responsible for the high degree of canting in **Bip**Pt(oligo) adducts. Instead, the H bonding of one G* O6 plays a greater role in the process whereby the carrier ligand affects the direction and degree of canting. Furthermore, for (*S,R,R,S*)-**Bip**Pt(oligo) adducts the 5′-X residue sugar has S pucker. These new results reinforce recent proposals dependent on related findings with ss less dynamic models. R canting and X sugar N pucker are required in duplexes for minimizing X base clashes with bases in the complementary strand and for favorable WC hydrogen-bonding and stacking interactions. These interactions, in turn, lead to the unusual characteristics of the XG* bp step.

For (*S,R,R,S*)-**Bip**Pt(oligo) adducts, when the oligo had a 5′-substituent (including a phosphate group), the HH1 conformer clearly dominated. This finding differs dramatically from results found for (*S,R,R,S*)-**Bip**Pt(d(G*pG*)) and (*S,R,R,S*)-**Bip**Pt(oligo) adducts lacking a 5′-residue; at equilibrium these adducts have substantial amounts of the ΔHT1 conformer in addition to the HH1 conformer. Given the diverse features of carrier ligands used in this and previous studies, there is no reason to believe that carrier-ligand to 5′-substituent interactions (such as hydrogen bonding) stabilize the HH1 conformer or that carrier-ligand to 5′-substituent steric clashes destabilize the ΔHT1 conformer. Rather, it is highly probable that the 5′-substituent steric clashes with the 3′-G* residue destabilize the ΔHT1 conformer.

Finally, our data provide insight into the probable conformer distribution in dynamic *cis*-Pt$(NH_3)_2$ ss adducts. From an analysis of our present findings and re-evaluation of previously studied *cis*-Pt$(NH_3)_2$(oligo) ss adducts,[23,45−47,67,69] we conclude that dynamic *cis*-Pt$(NH_3)_2$(oligo) ss adducts with a 5′-residue flanking the G*G* cross-link exist almost exclusively as the HH1 conformer. In the absence of a 5′-flanking residue,[47] such adducts are undoubtedly a mixture of rapidly interchanging abundant conformers (∼33% ΔHT1 and ∼67% HH1). Thus, the compelling evidence in our study for the presence in ss adducts lacking a 5′-substituent of a substantial amount of the ΔHT1 conformer allows us to reach the important conclusion that there is really no behavioral dichotomy between adducts with linked guanine bases (thought to greatly favor HH conformers) and those with unlinked guanine bases (thought to greatly favor HT conformers).

■ ASSOCIATED CONTENT

Supporting Information. Complete description of ^{1}H NMR signal assignments for G* residues of (*S,R,R,S*)-**Bip**Pt-(oligo) adducts and discussion of structural features of observed conformers; table of G H8, T H6, and T CH_3 NMR shifts of free oligos; table of ^{1}H and ^{31}P NMR signal assignments for the ΔHT1 conformer of (*S,R,R,S*)-**Bip**Pt(oligo) adducts; table of ^{1}H NMR signal assignments for the T residues of conformers for (*S,R,R,S*)-**Bip**Pt(oligo) adducts; table of ^{13}C NMR shifts for (*S,R,R,S*)-**Bip**Pt(oligo) adducts; table of ^{1}H and ^{31}P NMR shifts of previous ss Pt−oligo models; figures of the H8 region of ^{1}H NMR spectra of various adducts as a function of time; 2D NOESY spectrum of (*S,R,R,S*)-**Bip**Pt(d(TG*G*T)); and ^{1}H NMR spectra of (*S,R,R,S*)-**Bip**Pt(d(TTTG*G*)) as a function of temperature. This material is available free of charge via the Internet at http://pubs.acs.org.

■ AUTHOR INFORMATION

Corresponding Author

*Phone: 205-996-9282 (J.S.S.); 225-578-0933 (L.G.M.). Fax: 205-996-4008 (J.S.S.); 225-578-3463 (L.G.M.). E-mail: saad@uab.edu (J.S.S.); lmarzil@lsu.edu (L.G.M.).

Present Addresses

[||] Department of Microbiology, University of Alabama at Birmingham, 845 19th Street South, Birmingham, Alabama 35294, United States.

■ ACKNOWLEDGMENT

This investigation was supported by the UAB Comprehensive Cancer Center (to J.S.S.), by LSU (to L.G.M.), and by EC (COST Action D39) and the University of Bari (to G.N.). L.G.M. thanks the RAYMOND F. SCHINAZI INTERNATIONAL EXCHANGE PROGRAMME between the University of Bath, UK, and Emory University, Atlanta, GA, USA, for a Faculty Fellowship.

■ REFERENCES

(1) Lippert, B. *Cisplatin. Chemistry and Biochemistry of a Leading Anticancer Drug*; Wiley-VCH: Weinheim, 1999.
(2) Malina, J.; Novakova, O.; Vojtiskova, M.; Natile, G.; Brabec, V. *Biophys. J.* **2007**, *93*, 3950–3962.
(3) Reedijk, J. *Eur. J. Inorg. Chem.* **2009**, *10*, 1303–1312.
(4) Beljanski, V.; Villanueva, J. M.; Doetsch, P. W.; Natile, G.; Marzilli, L. G. *J. Am. Chem. Soc.* **2005**, *127*, 15833–15842.
(5) Bhattacharyya, D.; Marzilli, P. A.; Marzilli, L. G. *Inorg. Chem.* **2005**, *44*, 7644–7651.
(6) Chaney, S. G.; Campbell, S. L.; Temple, B.; Bassett, E.; Wu, Y.; Faldu, M. *J. Inorg. Biochem.* **2004**, *98*, 1551–1559.
(7) Kaspárková, J.; Vojtiskova, M.; Natile, G.; Brabec, V. *Chem.—Eur. J.* **2008**, *14*, 1330–1341.
(8) Natile, G.; Marzilli, L. G. *Coord. Chem. Rev.* **2006**, *250*, 1315–1331.
(9) Ober, M.; Lippard, S. J. *J. Am. Chem. Soc.* **2008**, *130*, 2851–2861.
(10) Ohndorf, U.-M.; Lippard, S. J. In *DNA Damage Recognition*; Siede, W., Kow, Y. W., Doetsch, P. W., Eds.; CRC: London, 2006; Vol. 12, pp 239−261.
(11) Sherman, S. E.; Gibson, D.; Wang, A.; Lippard, S. J. *J. Am. Chem. Soc.* **1988**, *110*, 7368–7381.
(12) Sherman, S. E.; Gibson, D.; Wang, A. H.-J.; Lippard, S. J. *Science* **1985**, *230*, 412–417.
(13) Ano, S. O.; Kuklenyik, Z.; Marzilli, L. G. In *Cisplatin. Chemistry and Biochemistry of a Leading Anticancer Drug*; Lippert, B., Ed.; Wiley-VCH: Basel, 1999, pp 247−291.
(14) Marzilli, L. G.; Saad, J. S.; Kuklenyik, Z.; Keating, K. A.; Xu, Y. *J. Am. Chem. Soc.* **2001**, *123*, 2764–2770.
(15) Ohndorf, U.-M.; Rould, M. A.; He, Q.; Pabo, C. O.; Lippard, S. J. *Nature* **1999**, *399*, 708–712.
(16) Lovejoy, K. S.; Todd, R. C.; Zhang, S.; McCormick, M. S.; D'Aquino, J. A.; Reardon, J. T.; Sancar, A.; Giacomini, K. M.; Lippard, S. J. *Proc. Natl. Acad. Sci. U.S.A.* **2008**, *105*, 8902–8907.
(17) Todd, R. C.; Lippard, S. J. In *Platinum and Other Heavy Metal Compounds in Cancer Chemotherapy*; Bonetti, A., Leone, R., Muggia, F. M., Howell, S. B., Eds.; Humana Press: New York, 2009; pp 67−72.
(18) Bloemink, M. J.; Reedijk, J. In *Metal Ions in Biological Systems*; Sigel, A., Sigel, H., Eds.; Marcel Dekker, Inc.: New York, 1996; Vol. 32, pp 641−685.
(19) Saad, J. S.; Natile, G.; Marzilli, L. G. *J. Am. Chem. Soc.* **2009**, *131*, 12314–12324.
(20) Sullivan, S. T.; Saad, J. S.; Fanizzi, F. P.; Marzilli, L. G. *J. Am. Chem. Soc.* **2002**, *124*, 1558–1559.
(21) Kline, T. P.; Marzilli, L. G.; Live, D.; Zon, G. *J. Am. Chem. Soc.* **1989**, *111*, 7057–7068.
(22) Yang, D.; van Boom, S.; Reedijk, J.; van Boom, J.; Wang, A. *Biochemistry* **1995**, *34*, 12912–12920.
(23) Girault, J.-P.; Chottard, G.; Lallemand, J.-Y.; Chottard, J.-C. *Biochemistry* **1982**, *21*, 1352–1356.
(24) Kozelka, J.; Fouchet, M. H.; Chottard, J.-C. *Eur. J. Biochem.* **1992**, *205*, 895–906.
(25) Admiraal, G.; van der Veer, J. L.; de Graaff, R. A. G.; den Hartog, J. H. J.; Reedijk, J. *J. Am. Chem. Soc.* **1987**, *109*, 592–594.
(26) Ano, S. O.; Intini, F. P.; Natile, G.; Marzilli, L. G. *J. Am. Chem. Soc.* **1998**, *120*, 12017–12022.
(27) Marzilli, L. G.; Ano, S. O.; Intini, F. P.; Natile, G. *J. Am. Chem. Soc.* **1999**, *121*, 9133–9142.
(28) Williams, K. M.; Cerasino, L.; Natile, G.; Marzilli, L. G. *J. Am. Chem. Soc.* **2000**, *122*, 8021–8030.
(29) Sullivan, S. T.; Ciccarese, A.; Fanizzi, F. P.; Marzilli, L. G. *J. Am. Chem. Soc.* **2001**, *123*, 9345–9355.
(30) Dijt, F. J.; Canters, G. W.; den Hartog, J. H.; Marcelis, A.; Reedijk, J. *J. Am. Chem. Soc.* **1984**, *106*, 3644–3647.
(31) Cramer, R. E.; Dahlstrom, P. L. *J. Am. Chem. Soc.* **1979**, *101*, 3679–3681.
(32) den Hartog, J. H. J.; Altona, C.; Chottard, J.-C.; Girault, J.-P.; Lallemand, J.-Y.; de Leeuw, F. A.; Marcelis, A. T. M.; Reedijk, J. *Nucleic Acids Res.* **1982**, *10*, 4715–4730.
(33) Sherman, S. E.; Lippard, S. J. *Chem. Rev.* **1987**, *87*, 1153–1181.
(34) Chottard, J. C.; Girault, J. P.; Chottard, G.; Lallemand, J. Y.; Mansuy, D. *J. Am. Chem. Soc.* **1980**, *102*, 5565–5572.
(35) Ano, S. O.; Intini, F. P.; Natile, G.; Marzilli, L. G. *Inorg. Chem.* **1999**, *38*, 2989–2999.
(36) Marzilli, L. G.; Intini, F. P.; Kiser, D.; Wong, H. C.; Ano, S. O.; Marzilli, P. A.; Natile, G. *Inorg. Chem.* **1998**, *37*, 6898–6905.
(37) Wong, H. C.; Coogan, R.; Intini, F. P.; Natile, G.; Marzilli, L. G. *Inorg. Chem.* **1999**, *38*, 777–787.
(38) Wong, H. C.; Intini, F. P.; Natile, G.; Marzilli, L. G. *Inorg. Chem.* **1999**, *38*, 1006–1014.
(39) Sullivan, S. T.; Ciccarese, A.; Fanizzi, F. P.; Marzilli, L. G. *Inorg. Chem.* **2000**, *39*, 836–842.
(40) Sullivan, S. T.; Ciccarese, A.; Fanizzi, F. P.; Marzilli, L. G. *Inorg. Chem.* **2001**, *40*, 455–462.
(41) Ano, S. O.; Intini, F. P.; Natile, G.; Marzilli, L. G. *J. Am. Chem. Soc.* **1997**, *119*, 8570–8571.
(42) Saad, J. S.; Benedetti, M.; Natile, G.; Marzilli, L. G. *Inorg. Chem.* **2011**, *50*, 4559–4571.
(43) Saad, J. S.; Scarcia, T.; Shinozuka, K.; Natile, G.; Marzilli, L. G. *Inorg. Chem.* **2002**, *41*, 546–557.
(44) Maheshwari, V.; Marzilli, P. A.; Marzilli, L. G. *Inorg. Chem.* **2011**, *50*, 6626–6636.

(45) den Hartog, J. H. J.; Altona, C.; van der Marel, G. A.; Reedijk, J. *Eur. J. Biochem.* **1985**, *147*, 371–379.
(46) Neumann, J.-M.; Tran-Dinh, S.; Girault, J.-P.; Chottard, J.-C.; Huynh-Dinh, T.; Igolen, J. *Eur. J. Biochem.* **1984**, *141*, 465–472.
(47) Fouts, C. S.; Marzilli, L. G.; Byrd, R.; Summers, M. F.; Zon, G.; Shinozuka, K. *Inorg. Chem.* **1988**, *27*, 366–376.
(48) Delaglio, F.; Grzesiek, S.; Vuister, G. W.; Zhu, G.; Pfeifer, J.; Bax, A. *J. Biomol. NMR* **1995**, *6*, 277–293.
(49) Johnson, B. A.; Blevins, R. A. *J. Biomol. NMR* **1994**, *4*, 603–614.
(50) In *CRC Handbook of Biochemistry and Molecular Biology*, 3rd ed.; Fasman, G. D., Ed.; CRC Press, Inc.: Cleveland, 1975; Vol. 1, Nucleic Acids.
(51) Qu, Y.; Farrell, N. *J. Am. Chem. Soc.* **1991**, *113*, 4851–4857.
(52) Berners-Price, S. J.; Ranford, J. D.; Sadler, P. *J. Inorg. Chem.* **1994**, *33*, 5842–5846.
(53) Mukundan, S., Jr.; Xu, Y.; Zon, G.; Marzilli, L. G. *J. Am. Chem. Soc.* **1991**, *113*, 3021–3027.
(54) van der Veer, J. L.; van der Marel, G. A.; van den Elst, H.; Reedijk, J. *Inorg. Chem.* **1987**, *26*, 2272–2275.
(55) Wüthrich, K. *NMR of Proteins and Nucleic Acids*; John Wiley & Sons: New York, 1986.
(56) Saenger, W. *Principles of Nucleic Acid Structure*; Springer-Verlag: New York, 1984.
(57) Kaspárková, J.; Mellish, K. J.; Qu, Y.; Brabec, V.; Farrell, N. *Biochemistry* **1996**, *35*, 16705–16713.
(58) Patel, D. J.; Kozlowski, S. A.; Nordheim, A.; Rich, A. *Proc. Natl. Acad. Sci. U.S.A.* **1982**, *79*, 1413–1417.
(59) Oda, Y.; Uesugi, S.; Ikehara, M.; Nishimura, S.; Kawase, Y.; Ishikawa, H.; Inoue, H.; Ohtsuka, E. *Nucleic Acids Res.* **1991**, *19*, 1407–1412.
(60) Ikehara, M.; Uesugi, S.; Yoshida, K. *Biochemistry* **1972**, *11*, 830–836.
(61) Iwamoto, M.; Mukundan, S., Jr.; Marzilli, L. G. *J. Am. Chem. Soc.* **1994**, *116*, 6238–6244.
(62) Wang, Y.; de los Santos, C.; Gao, X.; Greene, K. L.; Live, D. H.; Patel, D. J. *J. Mol. Biol.* **1991**, *222*, 819–832.
(63) Villanueva, J. M.; Jia, X.; Yohannes, P. G.; Doetsch, P. W.; Marzilli, L. G. *Inorg. Chem.* **1999**, *38*, 6069–6080.
(64) Carlone, M.; Fanizzi, F. P.; Intini, F. P.; Margiotta, N.; Marzilli, L. G.; Natile, G. *Inorg. Chem.* **2000**, *39*, 634–641.
(65) Elizondo-Riojas, M.-A.; Kozelka, J. *Inorg. Chim. Acta* **2000**, *297*, 417–420.
(66) Sundquist, W.; Lippard, S. J. *Coord. Chem. Rev.* **1990**, *100*, 293–322.
(67) van Garderen, C. J.; Bloemink, M. J.; Richardson, E.; Reedijk, J. *J. Inorg. Biochem.* **1991**, *42*, 199–205.
(68) Bloemink, M. J.; Heetebrij, R. J.; Inagaki, K.; Kidani, Y.; Reedijk, J. *Inorg. Chem.* **1992**, *31*, 4656–4661.
(69) Bloemink, M. J.; Perez, J. M. J.; Heetebrij, R. J.; Reedijk, J. *J. Biol. Inorg. Chem.* **1999**, *4*, 554–567.
(70) Sullivan, S. T.; Marzilli, L. G. Unpublished work.